Polarizable Anionic Sublattices Can Screen Molecular Dipoles in Noncentrosymmetric Inorganic−Organic Hybrids

Megan A. Cassingham, Yang G. Goh, Eric T. McClure, Taylor L. Hodgkins, Weiguo Zhang, Mingli Liang, Jahan M. Dawlaty, Peter I. Djurovich, Ralf Haiges, P. Shiv Halasyamani, Christopher N. Savory, Mark E. Thompson, and Brent C. Melot*

Cite This: https://doi.org/10.1021/acsami.2c20648

Read Online

ACCESS | Metrics & More | Article Recommendations | SI Supporting Information

ABSTRACT: We report the growth and photophysical characterization of two polar hybrid lead halide phases, methylenedianiline lead iodide and bromide, $(MDA)Pb_2I_6$ and $(MDA)Pb_2Br_6$, respectively. The phases crystallize in noncentrosymmetric space group $Fdd2$, which produces a highly oriented molecular dipole moment that gives rise to second harmonic generation (SHG) upon excitation at 1064 nm. While both compositions are isostructural, the size dependence of the SHG signal suggests that the bromide exhibits a stronger phase-matching response whereas the iodide exhibits a significantly weaker non-phase-matching signal. Similarly, fluorescence from $(MDA)Pb_2Br_6$ is observed around 630 nm below 75 K whereas only very weak luminescence from $(MDA)Pb_2I_6$ can be seen. We attribute the contrasting optical properties to differences in the character of the halide sublattice and postulate that the increased polarizability of the iodide ions acts to screen the local dipole moment, effectively reducing the local electric field in the crystals.

KEYWORDS: inorganic−organic hybrid, nonlinear optics, second harmonic generation, solid-state emission, polarizability
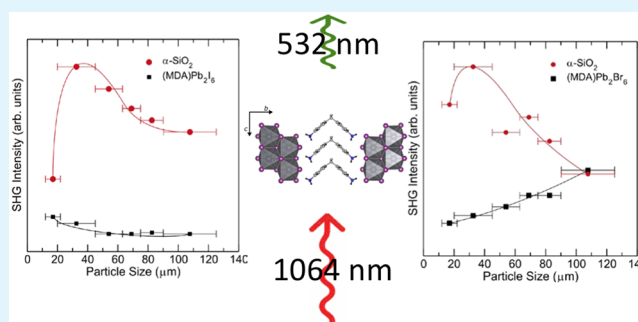
INTRODUCTION

The past decade has seen numerous studies of hybrid metal halide perovskites due to their high tolerance to defects, solution processability, and optoelectronic properties,[1−4] with the vast majority of attention focused on three-dimensional structures, like that of $CH_3NH_3PbI_3$.[5] While these phases exhibit exceptional photovoltaic performance, their functionality can be largely attributed to the inorganic portion of the hybrid,[6−8] with the organic molecules serving primarily as structural building blocks. Attempts to introduce organic moieties with optical properties in the more desirable visible range have demonstrated that the increased size typically required to achieve these properties results in crystal structures with reduced dimensionality in the inorganic connectivity through sheet and chain-like topologies.[5,9−12] While the reduced connectivity between the metals and ligands in these phases makes them less attractive for photovoltaic applications, in which high charge-carrier mobility is required, the ability to precisely control the separation between the HOMO and LUMO levels as well as the geometric shape of the molecules offers a promising avenue for tailoring the functionality of these materials.[8,12−16]

Herein, we investigate a pair of hybrids based on 4,4′-methylenedianiline ($C_{13}H_{14}N_2$, MDA), chosen for its strong intrinsic dipole, in which the organic cations crystallize in a chevron-like pattern to create a strongly coherent dipole that breaks the inversion symmetry of the structure to produce a polar material. We report the structure for the novel material, $(MDA)Pb_2Br_6$, and compare it to that of the iodide analogue, $(MDA)Pb_2I_6$, first reported by Lemmerer and Billing.[9] Weak SHG activity is observed in both the iodide, $(MDA)Pb_2I_6$, and the bromide, $(MDA)Pb_2Br_6$, confirming the assignment of a polar space group, but neither exhibits strong luminescence at room temperature. Upon cooling, polycrystalline powders of the bromide exhibit an emission centered around 630 nm while the iodide shows only very faint emission at the lowest temperatures. Using density functional theory (DFT) calculations and temperature-dependent dielectric measurements, we examine the role of localized vibrations from the organic moieties in the luminescent lifetime and discuss the influence of the lattice polarizability on the optical properties.

ACS Publications

A

■ EXPERIMENTAL DETAILS

The organic precursors MDA·2HI and MDA·2HBr were first prepared by dissolving 0.1 g (0.50 mmol) of MDA in 5 mL of acetone; then 0.5 mL of 57 wt % (7.57 M) HI or 48 wt % (8.89 M) HBr was then added, and the mixture was stirred to combine. This solution was then transferred to a glass Petri dish and placed on a warm hot plate to evaporate the solvent.

Crystals of $(MDA)Pb_2I_6$ were grown following the procedure reported by Lemmerer and Billings.[9] First, 0.1 g (0.22 mmol) of lead(II) iodide $[PbI_2, 99.9985\%$ (metal basis), Alfa Aesar] and 0.055 g (0.28 mmol) of 4,4′-methylenedianiline (MDA, 97%, Sigma-Aldrich) were dissolved separately in 3 and 5 mL of hydroiodic acid [HI, 57 wt % (stabilized), Sigma Alrdich] in 2 and 8 dram scintillation vials, respectively. Each solution was stirred continuously while being heated to 110 °C in an aluminum bead bath placed atop a hot plate.

Once the solids were fully dissolved, the solution of lead iodide was added to that of the MDA, and the mixture was stirred while continuing to be heated. The solution was allowed to cool naturally to room temperature within the bead bath to encourage crystallization. The resulting crystals were subsequently collected via vacuum filtration and rinsed thoroughly with diethyl ether [≥98% (stabilized), VWR]. Samples were stored in a desiccator or Ar-filled glovebox to minimize degradation due to atmospheric exposure.

The synthesis of $(MDA)Pb_2Br_6$ was adapted from that of the iodide with substitution of lead(II) bromide $[PbBr_2, 99.998\%$ (metal basis), Alfa Aesar] and hydrobromic acid (HBr, 48 wt %, VWR). In contrast to the iodide, cooling to room temperature did not result in crystallization; therefore, diethyl ether was layered on top at room temperature, and the mixture was allowed to sit for at least 24 h. Attempts to make the chloride analogue did not yield an isostructural product and instead resulted in a slightly different polymorph that will be the subject of a later publication.

X-ray powder diffraction (XRD) was used to confirm the purity and composition of $(MDA)Pb_2I_6$ and $(MDA)Pb_2Br_6$. Samples were ground using an agate mortar and pestle and characterized with a Bruker D8 Advance powder diffractometer equipped with a Cu Kα radiation source and a LynxEye XET detector. Data was collected from 5° to 70° (2θ angles) with a 0.02° step size and 1 s per step. High-resolution synchrotron XRD data were collected using the mail-in program at beamline 11-BM at the Advanced Photon Source (APS), Argonne National Laboratory. Discrete detectors covering an angular 2θ range from −6° to 16° were scanned over a 34° 2θ range, with data points collected every 0.001° 2θ and a scan speed of 0.01 °/s. The resulting patterns were evaluated using Rietveld refinement as implemented in TOPAS-Academic version 6[17] and GSAS-II.[18] Single-crystal data for $(MDA)Pb_2Br_6$ were collected using a Bruker APEX diffractometer with a CCD area detector. Diffuse reflectance data were collected from 800 to 250 nm using a PerkinElmer Lambda 950 ultraviolet–visible–near-infrared spectrophotometer equipped with a 150 mm integrating sphere to determine the onset of absorption in powders diluted to 3 wt % in MgO and to approximate the optical band gap using the Kubelka–Munk transform.[19]

Approximately 2 g of $(MDA)Pb_2I_6$ and approximately 2 g $(MDA)Pb_2Br_6$ were ground and sieved into distinct particle size ranges (<20, 20−45, 45−63, 63−75, 75−90, and 90−125 μm) for the phase matching experiment. The respective powders were transferred to individual quartz tubes, and the tubes were sealed for measurement. Relevant comparisons with known SHG-active materials were made by grinding and sieving crystalline α-SiO$_2$ and potassium dihydrogen phosphate (KDP) into the same particle size ranges. The samples were excited using a Nd:YAG laser source with a 1064 nm output. Any light emitted at 532 nm was amplified via a photomultiplier tube and collected at a detector. No index matching fluid was used in the experiment.

Photoluminescence spectra of $(MDA)Pb_2Br_6$ and $(MDA)Pb_2I_6$ were collected using neat solid samples in a cryostat system as described below. Each sample was sandwiched between two 1 mm thick sapphire disks and excited with a 375 nm light-emitting diode. Steady-state emission spectra were collected from 4 to 290 K using a

Photon Technology International QuantaMaster model C-60SE spectrofluorimeter in tandem with a Janis model SHI-4-2 optical He cryostat equipped with a Lakeshore model 335 temperature controller. Excited-state lifetimes were evaluated from 4 to 150 K and determined by the time-correlated single-photon counting method (TCSPC) using an IBH Fluorocube instrument using a 372 nm pulsed diode for the $(MDA)Pb_2Br_6$ sample, whereas $(MDA)Pb_2I_6$ was not bright enough to evaluate its lifetime at any temperature.

Periodic DFT calculations were performed using the Vienna Ab Initio Simulation Package (VASP),[20−23] using the projector-augmented wave method to describe the interaction between core and valence electrons.[24] The density of states and band diagram plots were visualized using sumo.[25] Pb 5d electrons were included in the valence, and all pseudopotentials were scalar-relativistic. Due to the size of the unit cells, the functional of Perdew, Burke, and Ernzerhof adapted for solids (PBEsol)[26] was used for geometrical relaxation, while the functional of Heyd, Scuseria, and Ernzerhof (HSE06),[27,28] with the explicit inclusion of spin–orbit coupling (HSE06+SOC), was used for electronic structure calculations, including density of states and electronic band structure, performed using the PBEsol-relaxed structures. PBEsol and HSE06+SOC have been previously demonstrated to be highly accurate in the prediction of structural and electronic properties, respectively, of hybrid inorganic–organic materials.[3,29,30] The total energies of both bromide and iodide compounds were found to converge to within 1 meV per atom using a plane wave energy cutoff of 400 eV and a Γ-centered k-point mesh of 4 × 4 × 4. Geometry optimization was considered converged when the forces on each atom fell below 0.01 eV Å^{-1}, and the plane wave cutoff was increased to 560 eV during relaxation to avoid Pulay stress.

■ RESULTS AND DISCUSSION

The preparation described above yielded small yellow (iodide) or white (bromide) needle-like crystals, which differ slightly from those reported by Lemmerer and Billing for $(MDA)Pb_2I_6$, who noted their crystals adopted a plate-like habit.[9] Rietveld refinement[31] against synchrotron XRD scattering from ground crystals, shown in panels a and b of Figure 1, shows the bulk of the product is a highly pure single phase with the refined parameters listed in Tables S2 and S3.

The structure of the hybrid crystallizes in noncentrosymmetric space group $Fdd2$ (No. 43) and is illustrated from two different perspectives in the insets of panels a and b of Figure 1. The fully inorganic region consists of edge-sharing chains of lead-centered octahedra running along the c-axis with the MDA cations positioned between them and held in place through hydrogen bonding between the amine group and iodide ions. Interestingly, the molecules adopt a chevron-like configuration with the methylene bridge of each pointing in a coherent fashion along the c-axis, parallel to the inorganic chains, which creates an obvious macroscopic dipole running throughout the material. Such an ordered dipole within a polar space group should be expected to give rise to nonlinear optical signals, which will be revisited in detail below.

The calculated densities of states (DOSs) for $(MDA)Pb_2Br_6$ and $(MDA)Pb_2I_6$, shown in Figure 2, reveal a contribution from the lead halide octahedra to both the conduction and valence band edges. The MDA cations make a greater energy contribution to the valence band maximum in $(MDA)Pb_2Br_6$ than in $(MDA)Pb_2I_6$. As expected, the band gap energy for the bromide hybrid increases relative to that of the iodide hybrid with a direct band gap of 3.54 eV in $(MDA)Pb_2Br_6$ and a direct band gap of 2.69 eV in $(MDA)Pb_2I_6$. The lead 6s and bromine 4p/iodine 5p orbitals in both materials are at the top of the valence band, but the carbon 2p orbital is much closer to the band edge in $(MDA)Pb_2Br_6$. The lead 6p orbital sits at the
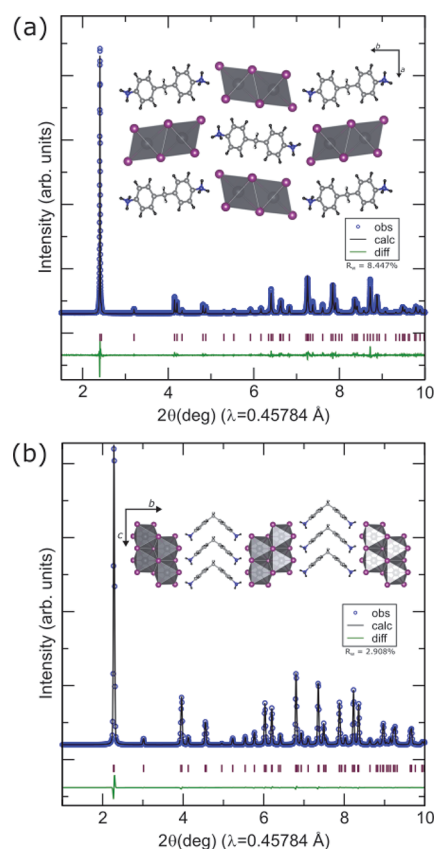
Figure 1. Results of the Rietveld refinement of the (a) $(MDA)Pb_2I_6$ and (b) $(MDA)Pb_2Br_6$ structures against synchrotron X-ray diffraction data collected on beamline 11-BM at Argonne National Laboratory.

Figure 2. Density of states for (a) $(MDA)Pb_2I_6$ and (b) $(MDA)-Pb_2Br_6$.

conduction band minimum with the carbon 2p orbital very close to the band edge in both hybrids.

Diffuse reflectance spectra in the ultraviolet−visible range were collected from powders of $(MDA)Pb_2I_6$, $(MDA)Pb_2Br_6$, PbI_2, $PbBr_2$, MDA·2HI, and MDA·2HBr to examine their optical properties. A Kubelka−Munk transformation was applied to each data set to estimate the optical band gap of each sample. Transforms for PbI_2, $PbBr_2$, MDA·2HI, and MDA·2HBr can be found in Figure S2. Figure 3 shows the Kubelka−Munk transforms for $(MDA)Pb_2I_6$ and $(MDA)-Pb_2Br_6$ along with insets of the bulk powder for each sample. The band gaps for $(MDA)Pb_2I_6$ and $(MDA)Pb_2Br_6$ are 2.65 and 2.90 eV, respectively, as determined by a linear fit to the onset of absorption. The absorption onsets for both PbI_2 and MDA·2HI were red-shifted compared to that of $(MDA)Pb_2I_6$, whereas the absorption onsets for $PbBr_2$ and MDA·2HBr were blue-shifted compared to that of $(MDA)Pb_2Br_6$.

$(MDA)Pb_2Br_6$ emits weakly at 595 nm at 290 K and strongly at 630 nm when cooled to 4 K (Figure 4), while $(MDA)Pb_2I_6$ emits only very weakly at temperatures below 80 K. In addition to the overall peak shape, the temperature dependencies of the principal emission band for bromide and iodide compounds show similar behavior. $(MDA)Pb_2I_6$ has an emission maximum of 620 nm at 4 K with a red shift to 628 nm at 75 K. At temperatures of ≤40 K, there is a clear peak at 450 nm that can be attributed to free exciton emission in $(MDA)Pb_2Br_6$. Figure S3 shows the complete emission profile that includes spectra at more temperatures, and Figure S4 shows the emission profile of $(MDA)Pb_2I_6$.
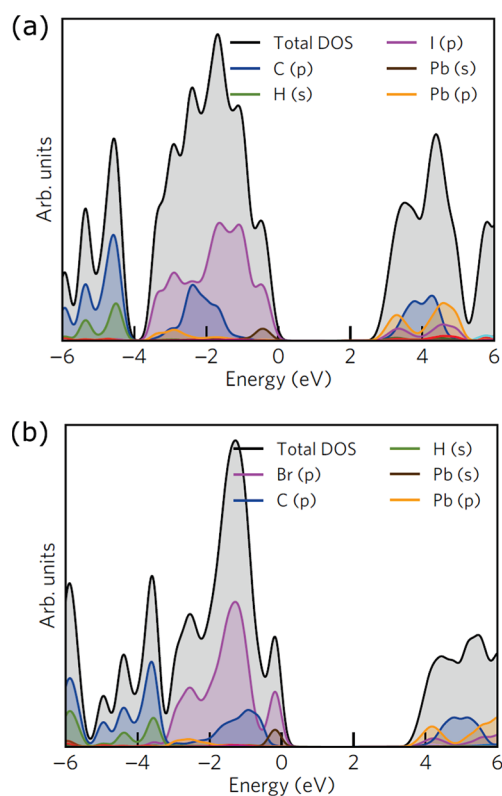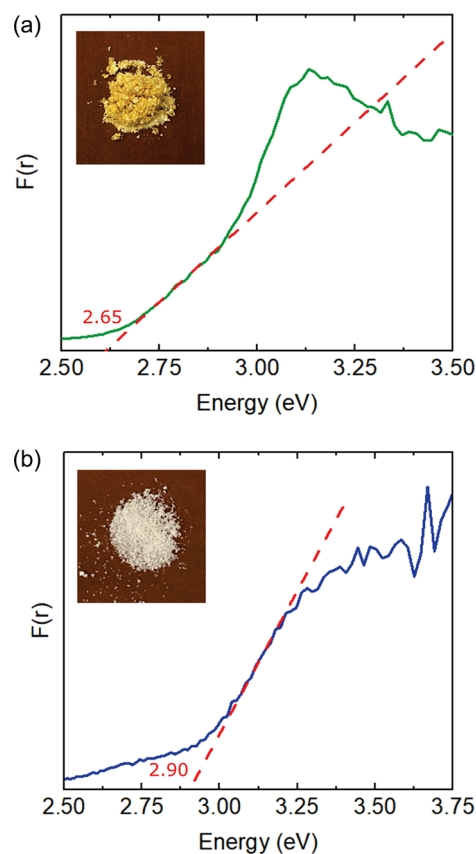

Figure 3. Kubelka−Munk transforms of (a) $(MDA)Pb_2I_6$ and (b) $(MDA)Pb_2Br_6$ with photos of the powders inset.
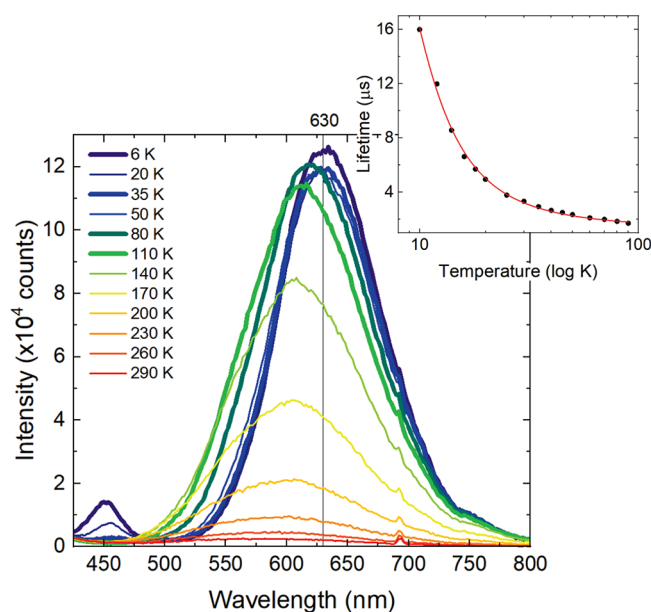
Figure 4. Variable-temperature emission of $(MDA)Pb_2Br_6$ from 4 to 290 K. The inset shows the $(MDA)Pb_2Br_6$ lifetime curve and fit from 10 to 90 K. Data were fit using a two-level model.

The lifetime data for $(MDA)Pb_2Br_6$ show that at low temperatures, the material is frozen into a state with a markedly longer lifetime as seen in the inset of Figure 4. The integrated intensities of the emission bands (replotted onto an axis of inverse centimeters) are constant in the range of 10−90 K (Table S1). It is unlikely that the radiative and nonradiative rates would have the same temperature dependence, so the changes in lifetime in this temperature regime are due to a decrease in the radiative rate at lower temperatures. Fitting of the lifetime data to an Arrhenius model (Figure 4 inset) gives an activation energy between the long- and short-lived states of 23 meV. Unfortunately, luminescence from $(MDA)Pb_2I_6$ is too weak to give accurate lifetime data, even at the lowest temperatures. Above 100 K, a nonradiative decay process(es) begins to compete with the radiative decay of the excited state, and the luminance efficiency decreases continuously to a photoluminescence quantum yield of <1% at room temperature for both compounds.

The polar nature of the space group encouraged us to investigate the nonlinear optical properties, which revealed SHG activity for both halides. When compared with that of α-SiO_2, the SHG intensity of $(MDA)Pb_2I_6$ is ~0.5 times as strong in the range of <20 μm, whereas the response for $(MDA)Pb_2Br_6$ is slightly larger in the range of 95−125 μm, with the iodide showing non-phase-matching behavior and the bromide showing phase-matching behavior as shown in Figure 5. A comparison of the phase-matching performance of $(MDA)Pb_2Br_6$ with KDP is also shown in Figure S5. It is curious, however, that despite what appears to be a substantial well-aligned molecular dipole, neither $(MDA)Pb_2I_6$ nor $(MDA)Pb_2Br_6$ displays a strong SHG intensity.

To better understand the polar nature of the material, temperature-dependent capacitance measurements were performed and are shown in Figure S1. The real part of the capacitance for both samples follows the typical dependence expected for a simple thermal contraction of the lattice upon cooling, and it is notable that there are no peaks or significant changes in slope, which rules out any ferroelectric transitions
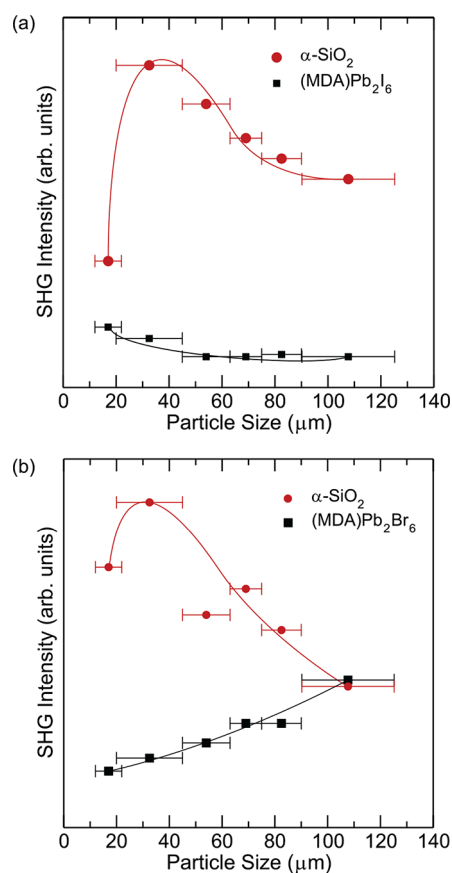

Figure 5. SHG phase matching curves of (a) $(MDA)Pb_2I_6$ and (b) $(MDA)Pb_2Br_6$ relative to α-SiO_2.

below room temperature. More interestingly, there appears to be a strong correlation between the evolution of luminescence in the two phases and features in the dielectric loss. We attribute this observation to a freezing of the rotation degrees of freedom on the ammonium portion of the MDA cations as previously described by Fabini et al.,[32,33] which would suppress a source of nonradiative quenching of the excited state and allow the observation of luminescence.

Aside from the weak SHG, there are no signatures in the dielectric properties to suggest that the ordered dipole on the MDA molecules introduces any novel functionality, which is somewhat surprising given the highly coherent alignment within the structure. We, therefore, postulate that the polarizability of the halide sublattice acts to screen the internal electric field created by these dipoles.[34] A recent report by Shen et al. offers deeper insight into this phenomenon. Their report on noncentrosymmetric morpholinium lead chloride and bromide systems shows phase-matching SHG effects of 0.70 and 0.81 times KDP, respectively, which would seem to contradict what is seen in the MDA hybrids.[12] However, in contrast to the materials we report, the dipole in their hybrids primarily arises from the acentric coordination environment of the metal halide octahedra. Therefore, while we believe the local electric field on the MDA molecules serves to polarize the charge cloud of the inorganic sublattice to produce a screening effect, the dipole of the morpholinium compounds is actually expected to increase in more polarizable lattices as this allows for greater displacement of lead from the center of its octahedra, in good agreement with their observations.

While the dielectric constant was difficult to evaluate at room temperature due to very high dielectric loss resulting from non-negligible electrical conductivity through the pellet, data collected at 2 K and 20 kHz indicate values of 11.0 and 8.3 for $(MDA)Pb_2Br_6$ and $(MDA)Pb_2I_6$, respectively. This supports the idea that the reduced polarizability of the $(MDA)Pb_2Br_6$ inhibits its ability to screen the internal electric field and allows it to exhibit a stronger SHG response.[35,36] This finding provides a powerful materials design principle for guiding the development of hybrids with polar or nonlinear optical properties and points toward chloride- and fluoride-based hybrids to ensure low electrical conductivity and small screening of any resulting electric fields.

■ CONCLUSION

In summary, we have demonstrated that $(MDA)Pb_2I_6$ and $(MDA)Pb_2Br_6$ both adopt noncentrosymmetric structures and, consequently, exhibit weak SHG activity. Counterintuitively, the dielectric constant of the iodide is weaker than that of the bromide, and as a result, the iodide shows a weaker SHG response. This behavior suggests that the increased polarizability of the iodide screens the ordered dipole on the MDA molecules. While neither material exhibits a ferroelectric transition, this trend in SHG activity may suggest that the design of polar hybrids should focus on chloride-based phases to maximize the attainable dipole moment.

■ ASSOCIATED CONTENT

ⓢ Supporting Information

The Supporting Information is available free of charge at https://pubs.acs.org/doi/10.1021/acsami.2c20648.

> Additional details of the crystallographic analysis, photophysics, and diffuse reflectance transforms and dielectric measurements (PDF)

■ AUTHOR INFORMATION

Corresponding Author

Brent C. Melot − *Department of Chemistry, University of Southern California, Los Angeles, California 90089, United States; Mork Family Department of Chemical Engineering and Materials Science, University of Southern California, Los Angeles, California 90089, United States;* ⓘ orcid.org/0000-0002-7078-8206; Email: melot@usc.edu

Authors

Megan A. Cassingham − *Department of Chemistry, University of Southern California, Los Angeles, California 90089, United States;* ⓘ orcid.org/0000-0001-7702-5511

Yang G. Goh − *Department of Chemistry, University of Southern California, Los Angeles, California 90089, United States;* ⓘ orcid.org/0000-0003-1086-4876

Eric T. McClure − *Department of Chemistry, University of Southern California, Los Angeles, California 90089, United States*

Taylor L. Hodgkins − *Department of Chemistry, University of Southern California, Los Angeles, California 90089, United States*

Weiguo Zhang − *Department of Chemistry, University of Houston, Houston, Texas 77204, United States*

Mingli Liang − *Department of Chemistry, University of Houston, Houston, Texas 77204, United States*

Jahan M. Dawlaty − *Department of Chemistry, University of Southern California, Los Angeles, California 90089, United States;* ⓘ orcid.org/0000-0001-5218-847X

Peter I. Djurovich − *Department of Chemistry, University of Southern California, Los Angeles, California 90089, United States;* ⓘ orcid.org/0000-0001-6716-389X

Ralf Haiges − *Department of Chemistry, University of Southern California, Los Angeles, California 90089, United States;* ⓘ orcid.org/0000-0003-4151-3593

P. Shiv Halasyamani − *Department of Chemistry, University of Houston, Houston, Texas 77204, United States;* ⓘ orcid.org/0000-0003-1787-1040

Christopher N. Savory − *Department of Chemistry and Thomas Young Centre, University College London, London WC1H 0AJ, United Kingdom;* ⓘ orcid.org/0000-0002-9052-7484

Mark E. Thompson − *Department of Chemistry, University of Southern California, Los Angeles, California 90089, United States;* ⓘ orcid.org/0000-0002-7764-4096

Complete contact information is available at: https://pubs.acs.org/10.1021/acsami.2c20648

Notes

The authors declare no competing financial interest.

■ ACKNOWLEDGMENTS

■ REFERENCES

(1) Snaith, H. J. Perovskites: The Emergence of a New Era for Low-Cost. *High-Efficiency Solar Cells* **2013**, *4*, 3623−3630.

(2) Zhang, W.; Eperon, G. E.; Snaith, H. J. Metal Halide Perovskites for Energy Applications. *Nat. Energy* **2016**, *1*, 16048.

(3) Yin, W.; Yang, J.; Kang, J.; Yan, Y.; Wei, S. Halide Perovskite Materials for Solar Cells: A Theoretical Review. *Journal of Materials Chemistry A* **2015**, *3*, 8926−8942.

(4) Brittman, S.; Adhyaksa, G. W. P.; Garnett, E. C. *Expanding World of Hybrid Perovskites: Materials Properties and Emerging Applications* **2015**, *5*, 7−26.

(5) Saparov, B.; Mitzi, D. B. *Organic-Inorganic Perovskites: Structural Versatility for Functional Materials Design* **2016**, *116*, 4558−4596.

(6) Wehrenfennig, C.; Eperon, G. E.; Johnston, M. B.; Snaith, H. J.; Herz, L. M. High Charge Carrier Mobilities and Lifetimes in Organolead Trihalide Perovskites. *Adv. Mater.* **2014**, *26*, 1584−1589.

(7) Ok, K. M.; Chi, E. O.; Halasyamani, P. S. Bulk Characterization Methods for Non-Centrosymmetric Materials: Second-Harmonic

Generation, piezoelectricity, pyroelectricity, and ferroelectricity. *Chem. Soc. Rev.* **2006**, *35*, 710−717.

(8) Su, B.; Song, G.; Molokeev, M. S.; Golovnev, N. N.; Lesnikov, M. K.; Lin, Z.; Xia, Z. Role of Metal-Chloride Anions in Photoluminescence Regulations for Hybrid Metal Halides. *J. Phys. Chem. Lett.* **2021**, *12*, 1918−1925.

(9) Lemmerer, A.; Billing, D. G. Lead Halide Inorganic-Organic Hybrids Incorporating Diammonium Cations. *CrystEngComm* **2012**, *14*, 1954−1966.

(10) Schmitt, T.; Bourelle, S.; Tye, N.; Soavi, G.; Bond, A. D.; Feldmann, S.; Traore, B.; Katan, C.; Even, J.; Dutton, S. E.; Deschler, F. Control of Crystal Symmetry Breaking with Halogen-Substituted Benzylammonium in Layered Hybrid Metal-Halide Perovskites. *J. Am. Chem. Soc.* **2020**, *142*, 5060−5067.

(11) Peng, Y.; Albero, J.; Álvarez, E.; García, H. Hybrid Benzidinium Lead Iodide Perovskites with a 1D Structure as Photoinduced Electron Transfer Photocatalysts. *Sustainable Energy & Fuels* **2019**, *3*, 2356−2360.

(12) Shen, C.; Sun, D.; Dang, Y.; Wu, K.; Xu, T.; Hou, R.; Chen, H.; Wang, J.; Wang, D. (C4H10NO)PbX3(X = Cl, Br): Design of Two Lead Halide Perovskite Crystals with Moderate Nonlinear Optical Properties. *Inorg. Chem.* **2022**, *61*, 16936−16943.

(13) Mitzi, D. B.; Chondroudis, K.; Kagan, C. Design, Structure, and Optical Properties of Organic-Inorganic Perovskites Containing an Oligothiophene Chromophore. *Inorg. Chem.* **1999**, *38*, 6246−6256.

(14) Stoumpos, C. C.; Malliakas, C. D.; Kanatzidis, M. G. Semiconducting Tin and Lead Iodide Perovskites with Organic Cations: Phase Transitions, High Mobilities, and Near-Infrared Photoluminescent Properties. *Inorg. Chem.* **2013**, *52*, 9019−9038.

(15) Trujillo-Hernández, K.; Rodríguez-López, G.; Espinosa-Roa, A.; González-Roque, J.; Gómora-Figueroa, A. P.; Zhang, W.; Halasyamani, P. S.; Jancik, V.; Gembicky, M.; Pirruccio, G.; Solis-Ibarra, D. Chirality control in white-light emitting 2D perovskites. *Journal of Materials Chemistry C* **2020**, *8*, 9602−9607.

(16) Yang, C.-K.; et al. The First 2D Homochiral Lead Iodide Perovskite Ferroelectrics: [R- and S-1-(4-Chlorophenyl)-ethylammonium]2PbI4. *Adv. Mater.* **2019**, *31*, 1808088.

(17) Coelho, A. A. *TOPAS* and *TOPAS-Academic*: An Optimization Program Integrating Computer Algebra and Crystallographic Objects Written in C++. *J. Appl. Crystallogr.* **2018**, *51*, 210−218.

(18) Toby, B. H.; Von Dreele, R. B. *GSAS-II*: The Genesis of a Modern Open-Source All Purpose Crystallography Software Package. *J. Appl. Crystallogr.* **2013**, *46*, 544−549.

(19) Kubelka, P.; Munk, F. An Article on Optics of Paint Layers. *Z. Phys.* **1931**, *12*, 593−601.

(20) Kresse, G.; Hafner, J. Ab Initio Molecular Dynamics for Liquid Metals. *Phys. Rev. B* **1993**, *47*, 558.

(21) Kresse, G.; Hafner, J. Ab Initio Molecular-Dynamics Simulation of the Liquid-Metal-Amorphous-Semiconductor Transition in Germanium. *Phys. Rev. B* **1994**, *49*, 14251.

(22) Kresse, G.; Furthmüller, J. Efficient Iterative Schemes for Ab Initio Total-Energy Calculations Using a Plane-Wave Basis Set. *Phys. Rev. B* **1996**, *54*, 11169−11186.

(23) Kresse, G.; Furthmüller, J. Efficiency of Ab Initio Total Energy Calculations for Metals and Semiconductors Using a Plane Wave Basis Set. *Comput. Mater. Sci.* **1996**, *6*, 15−50.

(24) Blochl, P. Projector Augmented-Wave Method. *Phys. Rev. B* **1994**, *50*, 17953−17979.

(25) Ganose, A. M.; Jackson, A. J.; Scanlon, D. O. sumo: Command-Line Tools for Plotting and Analysis of Periodic *ab initio* Calculations. *Journal of Open Source Software* **2018**, *3*, 717.

(26) Perdew, J. P.; Ruzsinszky, A.; Csonka, G. I.; Vydrov, O. A.; Scuseria, G. E.; Constantin, L. A.; Zhou, X.; Burke, K. Restoring the Density-Gradient Expansion for Exchange in Solids and Surfaces. *Phys. Rev. Lett.* **2008**, *100*, 136406.

(27) Heyd, J.; Scuseria, G. E.; Ernzerhof, M. Hybrid Functionals Based on a Screened Coulomb Potential. *J. Chem. Phys.* **2003**, *118*, 8207.

(28) Krukau, A. V.; Vydrov, O. A.; Izmaylov, A. F.; Scuseria, G. E. Influence of the Exchange Screening Parameter on the Performance of Screened Hybrid Functionals. *J. Chem. Phys.* **2006**, *125*, 224106.

(29) Bass, K. K.; Estergreen, L.; Savory, C. N.; Buckeridge, J.; Scanlon, D. O.; Djurovich, P. I.; Bradforth, S. E.; Thompson, M. E.; Melot, B. C. Structure in Room Temperature Photoluminescence of the Halide Perovskite Cs₃Bi₂Br₉. *Inorg. Chem.* **2017**, *56*, 42−45.

(30) Fabian, D. M.; Ganose, A. M.; Ziller, J. W.; Scanlon, D. O.; Beard, M. C.; Ardo, S. Influence of One Specific Carbon−Carbon Bond on the Quality, Stability, and Photovoltaic Performance of Hybrid Organic−Inorganic Bismuth Iodide Materials. *Applied Energy Materials* **2019**, *2*, 1579−1587.

(31) Rietveld, H. A Profile Refinement Method for Nuclear and Magnetic Structures. *J. Appl. Crystallogr.* **1969**, *2*, 65−71.

(32) Fabini, D. H.; Hogan, T.; Evans, H. A.; Stoumpos, C. C.; Kanatzidis, M. G.; Seshadri, R. Dielectric and Thermodynamic Signatures of Low-Temperature Glassy Dynamics in the Hybrid Perovskites CH3NH3PbI3 and HC(NH2)2PbI3. *J. Phys. Chem. Lett.* **2016**, *7*, 376−381.

(33) Fabini, D. H.; Siaw, T. A.; Stoumpos, C. C.; Laurita, G.; Olds, D.; Page, K.; Hu, J. G.; Kanatzidis, M. G.; Han, S.; Seshadri, R. Universal Dynamics of Molecular Reorientation in Hybrid Lead Iodide Perovskites. *J. Am. Chem. Soc.* **2017**, *139*, 16875−16884.

(34) Wilson, J. N.; Frost, J. M.; Wallace, S. K.; Walsh, A. Dielectric and Ferroic Properties of Metal Halide Perovskites. *APL Materials* **2019**, *7*, 010901.

(35) Kirkwood, J. G. On the Theory of Dielectric Polarization. *J. Chem. Phys.* **1936**, *4*, 592.

(36) Rumble, J. R. *CRC Handbook of Chemistry and Physics*, 102nd ed.; CRC Press, Francis and Taylor Group, 2021−2022, pp 10-188−10-189.